

This paper is published as part of a *Nanoscale* themed issue on [doped nanostructures](#)

Guest Editor: Stephen Pearton

Editorial

[Doped nanostructures](#)

Stephen Pearton, *Nanoscale*, 2010

DOI: [10.1039/c005273f](#)

Review Articles

[Impacts of doping on thermal and thermoelectric properties of nanomaterials](#)

Gang Zhang and Baowen Li, *Nanoscale*, 2010

DOI: [10.1039/c0nr00095g](#)

[Effect of N/B doping on the electronic and field emission properties for carbon nanotubes, carbon nanocones, and graphene nanoribbons](#)

Shan-Sheng Yu and Wei-Tao Zheng, *Nanoscale*, 2010

DOI: [10.1039/c0nr00002g](#)

[Silica-based nanoparticles for photodynamic therapy applications](#)

Pierre Couleaud, Vincent Morosini, Céline Frochot, Sébastien Richeter, Laurence Raehm and Jean-Olivier Durand, *Nanoscale*, 2010

DOI: [10.1039/c0nr00096e](#)

Mini Review

[Co-Doped ZnO nanoparticles: Minireview](#)

Igor Djerdj, Zvonko Jagličić, Denis Aržon and Markus Niederberger, *Nanoscale*, 2010

DOI: [10.1039/c0nr00148a](#)

Communications

[Controlling the volumetric parameters of nitrogen-doped carbon nanotube cups](#)

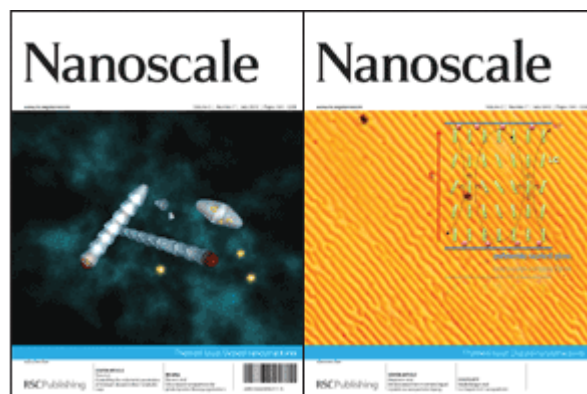
Brett L. Allen, Matthew B. Keddie and Alexander Star, *Nanoscale*, 2010

DOI: [10.1039/c0nr00043d](#)

[Visible light induced photobleaching of methylene blue over melamine-doped TiO₂ nanocatalyst](#)

Jurate Virkutyte, Babita Baruwati and Rajender S. Varma, *Nanoscale*, 2010

DOI: [10.1039/c0nr00089b](#)



[Selective detection of trace amount of Cu²⁺ using semiconductor nanoparticles in photoelectrochemical analysis](#)

Guang-Li Wang, Jing-Juan Xu and Hong-Yuan Chen, *Nanoscale*, 2010

DOI: [10.1039/c0nr00084a](#)

[Flower-like TiO₂ nanostructures with exposed {001} facets: Facile synthesis and enhanced photocatalysis](#)

Min Liu, Lingyu Piao, Weiming Lu, Siting Ju, Lei Zhao, Chunlan Zhou, Hailing Li and Wenjing Wang, *Nanoscale*, 2010

DOI: [10.1039/c0nr00050g](#)

Papers

[Electroconvection in nematic liquid crystals via nanoparticle doping](#)

Martin Urbanski, Brandy Kinkead, Hao Qi, Torsten Hegmann and Heinz-S. Kitzerow, *Nanoscale*, 2010

DOI: [10.1039/c0nr00139b](#)

[Superhydrophilicity-assisted preparation of transparent and visible light activated N-doped titania film](#)

Qing Chi Xu, Diana V. Wellia, Rose Amal, Dai Wei Liao, Say Chye Joachim Loo and Timothy Thatt Yang Tan, *Nanoscale*, 2010

DOI: [10.1039/c0nr00105h](#)

[The influence of doping on the device characteristics of In_{0.5}Ga_{0.5}As/GaAs/Al_{0.2}Ga_{0.8}As quantum dots-in-a-well infrared photodetectors](#)

G. Jolley, L. Fu, H. H. Tan and C. Jagadish, *Nanoscale*, 2010

DOI: [10.1039/c0nr00128g](#)

[Study of concentration-dependent cobalt ion doping of TiO₂ and TiO_{2-x}N_x at the nanoscale](#)

James L. Gole, Sharka M. Prokes, O. J. Glembocki, Junwei Wang, Xiaofeng Qiu and Clemens Burda, *Nanoscale*, 2010

DOI: [10.1039/c0nr00125b](#)

[Multifunctional nanocomposites of superparamagnetic \(Fe₃O₄\) and NIR-responsive rare earth-doped up-conversion fluorescent \(NaYF₄: Yb,Er\) nanoparticles and their applications in biolabeling and fluorescent imaging of cancer cells](#)

Congcong Mi, Jingpu Zhang, Huanyu Gao, Xianlong Wu, Meng Wang, Yingfan Wu, Yueqin Di, Zhangrun Xu, Chuanbin Mao and Shukun Xu, *Nanoscale*, 2010
DOI: [10.1039/c0nr00102c](#)

[Effect of doping on the morphology and multiferroic properties of BiFeO₃ nanorods](#)

Dimple P. Dutta, O. D. Jayakumar, A. K. Tyagi, K. G. Girija, C. G. S. Pillai and G. Sharma, *Nanoscale*, 2010
DOI: [10.1039/c0nr00100g](#)

[Effect of substrate temperature on implantation doping of Co in CdS nanocrystalline thin films](#)

S. Chandramohan, A. Kanjilal, S. N. Sarangi, S. Majumder, R. Sathyamoorthy, C.-H. Hong and T. Som, *Nanoscale*, 2010
DOI: [10.1039/c0nr00123f](#)

[Modification of neodymium-doped ZnO hybrid nanoparticles under mild hydrothermal conditions](#)

Behzad Shahmoradi, K. Soga, S. Ananda, R. Somashekar and K. Byrappa, *Nanoscale*, 2010
DOI: [10.1039/c0nr00069h](#)

[Ex situ vapor phase boron doping of silicon nanowires using BBr₃](#)

Gregory S. Doerk, Gabriella Lestari, Fang Liu, Carlo Carraro and Roya Maboudian, *Nanoscale*, 2010
DOI: [10.1039/c0nr00127a](#)

[Change in conformation of polymer PFO on addition of multiwall carbon nanotubes](#)

Malti Bansal, Ritu Srivastava, C. Lal, M. N. Kamalasanan and L. S. Tanwar, *Nanoscale*, 2010
DOI: [10.1039/c0nr00001a](#)

[Amino acid-assisted one-pot assembly of Au, Pt nanoparticles onto one-dimensional ZnO microrods](#)

Xianghong Liu, Jun Zhang, Xianzhi Guo, Shihua Wu and Shurong Wang, *Nanoscale*, 2010
DOI: [10.1039/c0nr00015a](#)

[Luminescence resonance energy transfer from an upconverting nanoparticle to a fluorescent phycobiliprotein](#)

Fiorenzo Vetrone, Rafik Naccache, Christopher G. Morgan and John A. Capobianco, *Nanoscale*, 2010
DOI: [10.1039/c0nr00126k](#)

[Doping single-walled carbon nanotubes through molecular charge-transfer: a theoretical study](#)

Arun K. Manna and Swapan K. Pati, *Nanoscale*, 2010
DOI: [10.1039/c0nr00124d](#)

[Energy transfer study between Ce³⁺ and Tb³⁺ ions in doped and core-shell sodium yttrium fluoride nanocrystals](#)

Pushpal Ghosh, Arik Kar and Amitava Patra, *Nanoscale*, 2010
DOI: [10.1039/c0nr00019a](#)

[Pt surface modification of SnO₂ nanorod arrays for CO and H₂ sensors](#)

Hui Huang, C. Y. Ong, J. Guo, T. White, M. S. Tse and O. K. Tan, *Nanoscale*, 2010
DOI: [10.1039/c0nr00159g](#)

[Poly \(acrylic acid\)-capped lanthanide-doped BaFCl nanocrystals: synthesis and optical properties](#)

Qiang Ju, Wenqin Luo, Yongsheng Liu, Haomiao Zhu, Renfu Li and Xueyuan Chen, *Nanoscale*, 2010
DOI: [10.1039/c0nr00116c](#)

[Enhanced Cu emission in ZnS: Cu,Cl/ZnS core-shell nanocrystals](#)

Carley Corrado, Morgan Hawker, Grant Livingston, Scott Medling, Frank Bridges and Jin Z. Zhang, *Nanoscale*, 2010
DOI: [10.1039/c0nr00056f](#)

[Synthesis and characterization of zirconium-doped mesoporous nano-crystalline TiO₂](#)

Kanattukara Vijayan Bineesh, Dong-Kyu Kim and Dae-Won Park, *Nanoscale*, 2010
DOI: [10.1039/c0nr00108b](#)

[Zn-doped nanocrystalline TiO₂ films for CdS quantum dot sensitized solar cells](#)

Guang Zhu, Zujun Cheng, Tian Lv, Likun Pan, Qingfei Zhao and Zhuo Sun, *Nanoscale*, 2010
DOI: [10.1039/c0nr00087f](#)

[Effect of synergy on the visible light activity of B, N and Fe co-doped TiO₂ for the degradation of MO](#)

Mingyang Xing, Yongmei Wu, Jinlong Zhang and Feng Chen, *Nanoscale*, 2010
DOI: [10.1039/c0nr00078g](#)

[Facile synthesis of lanthanide nanoparticles with paramagnetic, down- and up-conversion properties](#)

Zhengquan Li and Yong Zhang, *Nanoscale*, 2010
DOI: [10.1039/c0nr00073f](#)

[Glucose oxidase-doped magnetic silica nanostructures as labels for localized signal amplification of electrochemical immunosensors](#)

Jingjing Ren, Dianping Tang, Biling Su, Juan Tang and Guonan Chen, *Nanoscale*, 2010
DOI: [10.1039/b9nr00416e](#)

[The role of ellipticity on the preferential binding site of Ce and La in C₇₈-D_{3h}—A density functional theory study](#)

K. Muthukumar and J. A. Larsson, *Nanoscale*, 2010
DOI: [10.1039/c0nr00021c](#)

[Tuning the shape and thermoelectric property of PbTe nanocrystals by bismuth doping](#)

Qian Zhang, Ting Sun, Feng Cao, Ming Li, Minghui Hong, Jikang Yuan, Qingyu Yan, Huey Hoon Hng, Nianqiang Wu and Xiaogang Liu, *Nanoscale*, 2010
DOI: [10.1039/c0nr00115e](#)

Poly (acrylic acid)-capped lanthanide-doped BaFCl nanocrystals: synthesis and optical properties

Qiang Ju, Wenqin Luo, Yongsheng Liu, Haomiao Zhu, Renfu Li and Xueyuan Chen*

Received 14th February 2010, Accepted 15th March 2010

First published as an Advance Article on the web 19th May 2010

DOI: 10.1039/c0nr00116c

Water-soluble lanthanide-doped BaFCl nanophosphors with the surface functionalized by a layer of poly (acrylic acid) are synthesized *via* a facile one-step solvothermal method. Intense long-lived luminescence is realized from visible to near-infrared (NIR) by doping with different lanthanide ions. The emission and excitation spectra of Eu^{3+} indicate that the doped lanthanide ions occupy a site close to the surface of the nanoparticles. Strong NIR emissions of Nd^{3+} and green luminescence of Tb^{3+} using Ce^{3+} as sensitizers are also achieved in BaFCl nanoparticles. The synthesized nanoparticles featuring long-lived luminescence in either visible or NIR regions may have potential applications as luminescent labels for biological applications.

1. Introduction

The application of fluorescent labeling materials has greatly stimulated the study of complex biological interactions in the field of biology.^{1–5} The common fluorescent labeling materials such as organic dyes and quantum dots (QDs) have been applied in biological analyses.^{6,7} However, some limitations are inevitable for these kinds of materials. For example, most organic dyes exhibit weak photostability and broad emission bands, while various semiconducting QDs might suffer from potential toxicity, chemical instability, short luminescence lifetimes, or photoblinking. As an alternative to dyes and QDs, trivalent lanthanide (Ln^{3+}) doped nanoparticles have been proposed as a new class of biological fluorescent labeling due to their attractive optical and chemical features.^{8–10} First, they inherit the advantages of a rigid crystal environment for the doped Ln^{3+} ions. Second, the interference from spontaneous background emission sources can be avoided by utilizing the inherent long-lived luminescence lifetimes (μs – ms range). Moreover, the spectroscopic selectivity of the nanoparticles can be extended beyond the range of interferences from biological systems by means of doping with different Ln^{3+} ions. All these optical merits enable the material to be used as an excellent candidate in the biological field.

Generally, to achieve highly efficient radiative emissions of the Ln^{3+} ions, the competitive phonon-assisted non-radiative transitions should be inhibited to the utmost, which require a low phonon frequency host for the Ln^{3+} ions. BaFCl is such kind of material as a fluorescent host matrix owing to its low vibrational energies (294 cm^{-1}).¹¹ In addition, the stable physical and chemical properties of BaFCl, particularly in aqueous solution, facilitate its further application as biological labels. Recently, we have synthesized Eu^{3+} -doped BaFCl powders that yielded strong red emissions of Eu^{3+} .¹² Nevertheless, the obtained particles are

too large to be used as biological labels which require that the nanoparticles are small in size ($<50\text{ nm}$), possess hydrophilic properties and a modified surface to provide the anchoring sites for further linking with biomolecules.¹³ To date, various approaches have been applied to synthesize the monodispersed small size nanoparticles. However, most of them are non-hydrophilic and can not be directly applied in biological detection.¹⁴ Although the surface modification or lipid encapsulation can transfer the hydrophobic products from non-polar solvents to water and modify their surface with terminal groups (*e.g.*, carboxylic, amino, thiol/maleimide),^{15–18} they still suffer from problems including tedious procedures, unavoidable adsorption and random immobilization, and complicated experimental conditions. Therefore, a facile one-step synthesis of the small-size, water-soluble, and surface-functionalized nanoparticles under common experimental conditions, have attracted considerable interest in recent years.¹⁹ Water-soluble and biocompatible $\text{LaF}_3:\text{Eu}^{3+}$, Fe_3O_4 , and $\text{LaPO}_4:\text{Ce}^{3+}/\text{Tb}^{3+}$ nanoparticles have been prepared through a one-step route.^{20–23} To our knowledge, there is no report on the synthesis of water-soluble and surface-functionalized Ln^{3+} -doped BaFCl nanoparticles before this study.

Herein, we report on the synthesis of water-soluble and carboxylic acid functionalized BaFCl nanoparticles through a facile one-step solvothermal method with polyelectrolyte and poly (acrylic acid) (PAA) as a capping agent. By doping different Ln^{3+} ions, red (Eu^{3+}), green ($\text{Ce}^{3+}/\text{Tb}^{3+}$), and near-infrared (Nd^{3+}) emissions are obtained. These results reveal that Ln^{3+} -doped BaFCl nanoparticles might have potential applications as efficient luminescent labels for biological imaging and immunoassays.

2. Experimental

2.1. Sample preparation

The water-soluble and PAA-coated Ln^{3+} -doped BaFCl nanoparticles were synthesized by a solvothermal method. 0.9 g PAA (MW = 1800), 1 mmol $\text{BaCl}_2 \cdot 2\text{H}_2\text{O}$ and the required amount of

Key Laboratory of Optoelectronic Materials Chemistry and Physics, Fujian Institute of Research on the Structure of Matter, Chinese Academy of Sciences, Fuzhou, Fujian, 350002, China. E-mail: xchen@fjirsm.ac.cn; Fax: + 86 591 8764-2575; Tel: + 86 591 8764-2575

$\text{LnCl}_3 \cdot 6\text{H}_2\text{O}$ ($\text{Ln} = \text{Eu}, \text{Ce}, \text{Tb}, \text{Nd}$) were dissolved in 30 mL ethylene glycol and stirred at room temperature (RT) for several minutes to afford a transparent solution. Another solution of 1 mmol NH_4F in 10 mL ethylene glycol was then added dropwise to BaCl_2 solution. The mixed transparent solution was stirred for another 10 min, then transferred into a 50 mL autoclave and solvothermally heated at 180 °C for 10 h. After cooling to RT, the resulting solution was acidified with dilute HCl solution, and centrifuged at 9000 r/min for 4 min to separate the solid powder products. The crude precipitate was continuously washed several times with distilled water and absolute ethanol in turn, and dried under vacuum at 50 °C for 4 h to yield the white final products.

2.2. Characterization

The powder X-ray diffraction (XRD) pattern of the sample was measured using a PANalytical X'Pert PRO powder diffractometer with $\text{Cu-K}\alpha 1$ radiation ($\lambda = 0.154 \text{ nm}$). The morphology and chemical compositions of the sample were investigated by a JEOL-2010 transmission electron microscope (TEM) equipped with the energy dispersive X-ray spectrum (EDS). Fourier transform infrared (FT-IR) spectra were recorded on a Magna 750 FT-IR spectrophotometer in the range of 400–4000 cm^{-1} . Thermal stability studies (30–1200 °C) were carried out on a NETSCHZ STA-449C thermoanalyzer under N_2 atmosphere at a heating rate of 10 °C min^{-1} . Emission and excitation spectra and transient decays were recorded on an Edinburgh Instruments FLS920 spectrofluorimeter equipped with both continuous (450 W) and pulsed xenon lamps. Laser spectroscopic measurements were carried out upon excitation by a mode-locked picosecond Ti:sapphire laser (700–1000 nm, pulse width $\leq 1.5 \text{ ps}$, Tsunami, Spectra-Physics) at RT. The near-infrared (NIR) decay was measured with a customized UV to mid-infrared steady-state and phosphorescence lifetime spectrometer (FSP920-C, Edinburgh) equipped with a digital oscilloscope (TDS3052B, Tektronix) and a tunable mid-band OPO pulse laser as the excitation source (410–2400 nm, 10 Hz, pulse width $\leq 5 \text{ ns}$, Vibrant 355II, OPOTEK). Photoluminescence (PL) photographs of the nanoparticles in aqueous solution were taken with Sony digital single lens reflex D100.

3. Results and discussion

3.1. Synthesis and structure characterization

Fig. 1(a) shows the XRD pattern of the as-obtained $\text{BaFCl}:\text{Eu}^{3+}$ nanoparticles, as well as the standard diffraction lines of tetragonal BaFCl crystals (JCPDS card No. 76-1368). The diffraction peaks of $\text{BaFCl}:\text{Eu}^{3+}$ (2 at.%) nanoparticles (the upper line) can be well indexed to the pure tetragonal BaFCl phase as shown in the bottom line of Fig. 1(a), and no trace of characteristic peaks was observed for other impurity phases such as BaF_2 or EuF_3 , showing that the one-step synthesis route is a feasible way for preparing pure phase BaFCl nanoparticles. The mean size of the nanoparticles was calculated to be $\sim 25 \text{ nm}$ by the Debye–Scherrer formula. As shown in the inset of Fig. 1(a), the BaFCl nanoparticles can be readily dispersed in water as a result of the PAA modification, which keep stable at the pH range from 4 to 14, similar to the previous report on PAA-capped Fe_3O_4 nanoparticles.²¹ From the TEM image

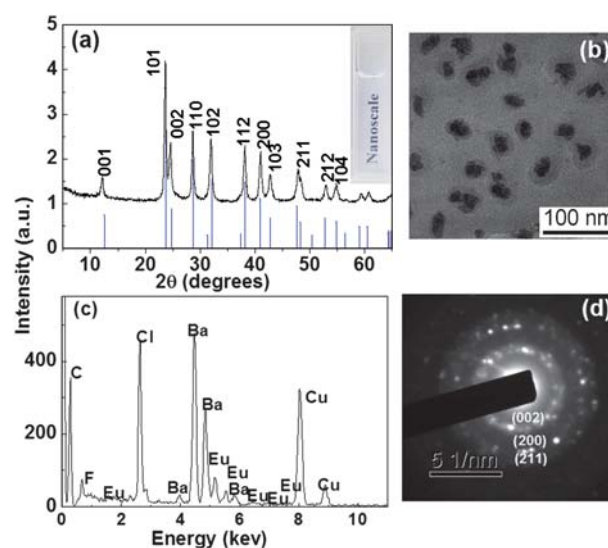


Fig. 1 (a) XRD pattern of $\text{BaFCl}:\text{Eu}^{3+}$ nanoparticles (the upper line) and standard data for tetragonal BaFCl crystals (JCPDS No. 76-1368, the bottom line); (b) TEM image, (c) EDS and (d) SAED patterns of $\text{BaFCl}:\text{Eu}^{3+}$ (2 at.%) nanoparticles. The inset of Fig. 1(a) is the photograph of BaFCl nanoparticles in aqueous solution.

(Fig. 1(b)), it can be seen that the $\text{BaFCl}:\text{Eu}^{3+}$ nanoparticles are roughly grain-like with the diameter ranging from 20–40 nm. Noticeably, there is a clear layer with a thickness of 5–15 nm capping on the nanoparticles, which is attributed to the PAA coating. There was little change in the surface layer even after it was washed ten times with absolute ethanol, showing strong combination of PAA onto the nanoparticles. The selected area electron diffraction (SAED) rings in Fig. 1(d) exhibit the polycrystalline nature of $\text{BaFCl}:\text{Eu}^{3+}$ nanoparticles, and can be indexed to diffractions from the (002), (200), and (211) planes of the tetragonal matlockite structure in turn, in accordance with the above XRD analysis. It should be mentioned that the nanoparticles doped with different Ln^{3+} ions exhibit essentially the same crystal phase and morphology. The EDS measurement (Fig. 1(c)) verifies the existence of Ba, F, Cl and Eu in $\text{BaFCl}:\text{Eu}^{3+}$ nanoparticles.

To further confirm the coating of PAA on the surface of nanoparticles, the FT-IR absorption spectra of both BaFCl nanoparticles and pure PAA were measured. As shown in Fig. 2(a), four peaks located at 2951, 1737, 1456 and 1407 cm^{-1} were observed in the pure PAA sample which can be assigned to characteristic absorption bands of PAA, corresponding to the stretching and bending modes of CH_2 , stretching modes of $\text{C}=\text{O}$ and $\text{C}-\text{O}$ in COOH group, respectively.²¹ For the BaFCl nanoparticles, these four peaks can also be observed, clearly indicating that a large amount of PAA was capped on the surfaces of the nanoparticles. Besides, a new distinguishable band at 1556 cm^{-1} was observed, which is attributed to the $\text{C}-\text{O}$ stretching mode of carboxylic groups deriving from the COO^- groups that coordinate to cations (*i.e.*, Ba^{2+}) on the surface of BaFCl nanoparticles. As schematically illustrated in Fig. 3, the carboxylic groups on the PAA chains strongly coordinate to Ba^{2+} on the nanoparticle surface to form a robust coating, while uncoordinated carboxylic groups extend into the aqueous solution, endowing the nanoparticles with high dispersibility in

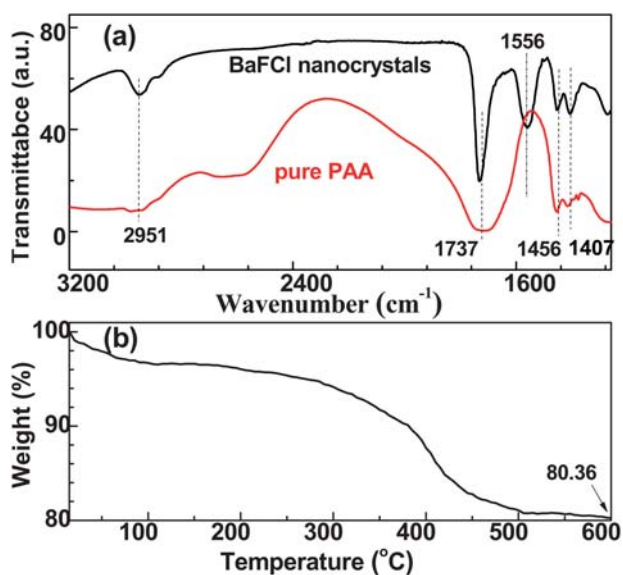


Fig. 2 (a) FT-IR spectra of PAA-capped BaFCl nanoparticles (black) and pure PAA (red); (b) thermogravimetric curve of PAA-capped BaFCl nanoparticles.

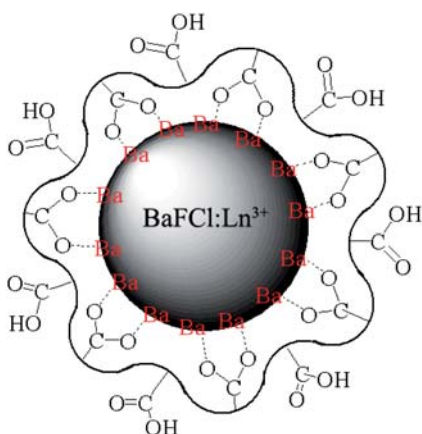


Fig. 3 Schematic illustration of PAA-coated BaFCl nanoparticles. Partial carboxylic groups bind to the nanoparticle surface and the others extend into the surrounding water, rendering the nanoparticles water-soluble.

water. Meanwhile, a large number of uncoordinated carboxylic groups on the nanoparticle surfaces can be used for the further conjugation of biomolecules. To investigate the PAA coating efficiency, thermogravimetric analysis was conducted. As shown in Fig. 2(b), the weight loss of ~ 4 wt.% in the initial step from 30 to 200 °C resulted from the evaporation of water and other solvent residuals, while the major weight loss of ~ 16 wt.% ranging from 200 to 600 °C was induced by the decomposition of PAA, in agreement with previous reports.^{18,24} The mass losses confirm the surface functionalization of PAA on BaFCl nanoparticles.

3.2. Optical properties

3.2.1. BaFCl:Eu³⁺. Due to the smaller size of BaFCl:Ln³⁺ nanoparticles and PAA modification, the PL spectra and

dynamics of Ln³⁺ are expected to differ to some extent from that of the bulk or no surface-functionalized counterparts. To investigate such variations, Eu³⁺ ion was chosen as an optical probe because its luminescence is very sensitive to its immediate surroundings.¹¹ Under excitation at 394 nm, the emission spectrum of the BaFCl:Eu³⁺ (2 at.%) nanoparticles (Fig. 4(a)) was mainly located in the red spectral region. The characteristic emission bands of Eu³⁺ at 578.5, 590, 612, and 699 nm were assigned to the ⁵D₀ → ⁷F₀, ⁷F₁, ⁷F₂, and ⁷F₄ transitions, respectively. Only one peak for the ⁵D₀ → ⁷F₀ transition was observed as revealed in the inset of Fig. 4(a), indicating that all the emissions come from the Eu³⁺ ions in the same crystalline site because both ⁵D₀ and ⁷F₀ are non-degenerate.¹¹ Moreover, all the observed emission lines are only moderately resolved indicating that Eu³⁺ ions are very likely to be located at the distorted lattice site near the surface. The local symmetry of Eu³⁺ ions can be roughly estimated from the intensity ratio of ⁵D₀ → ⁷F₁ and ⁵D₀ → ⁷F₂ transitions.²⁵ The calculated intensity ratio is 0.8, similar to that of Eu³⁺ ions which sit at site A close to the surface with the site symmetry of C_{2v} or lower in a preceding report on BaFCl:Eu³⁺ powders,¹² which thus verifies that the Eu³⁺ dopant is mostly situated at the site close to the surface. In addition to the

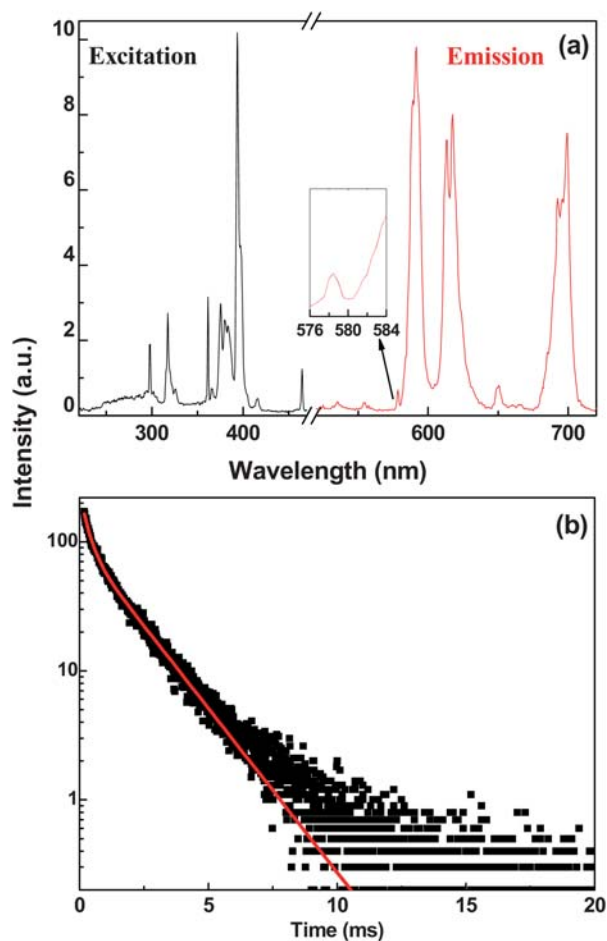


Fig. 4 (a) The excitation (left, $\lambda_{em} = 591$ nm) and emission (right, $\lambda_{ex} = 394$ nm) spectra and (b) decay curve of BaFCl:Eu³⁺ (2 at.%) nanoparticles in aqueous solution. The inset of Fig. 4(a) enlarges the spectral region of the ⁵D₀ → ⁷F₀ transition at 578.5 nm.

emissions from 5D_0 , some weak emission lines from the higher excited state of 5D_1 were also observed, owing to the very low phonon frequencies of BaFCl nanoparticles.¹¹ In the excitation spectrum by monitoring the $^5D_0 \rightarrow ^7F_1$ transition at 591 nm (Fig. 4(a)), the characteristic excitation bands of Eu^{3+} were observed from the energy levels of 5F_5 at 298 nm, $^5H_{3-7}$ at 317 nm, 5D_4 at 361 nm, 5G_6 at 376 nm, 5G_2 at 380 nm, 5L_6 at 397 nm, 5D_3 at 414 nm, and 5D_2 at 464 nm, among which the most intense excitation line is peaked at 397 nm.

Fig. 4(b) shows the luminescence decay of Eu^{3+} by monitoring the $^5D_0 \rightarrow ^7F_1$ transition at 591 nm under the direct excitation to the 5L_6 state at 394 nm. The luminescence decay of 5D_0 deviates significantly from a single exponential function, which is presumably due to the energy transfer process from Eu^{3+} to the neighboring surface defects, very different from the observation for larger nanocrystals previously reported.¹² The decay curve was fitted with double exponential function, giving rise to a longer lifetime of 1.70 ms (78%) and a shorter one of 0.29 ms (22%). The longer lifetime is slightly larger than that of BaFCl: Eu^{3+} nanopowders (1.4 ms for Eu^{3+} at site A close to the surface in aqueous solution), which may be caused by the smaller effective index of refraction for smaller particles as often observed in Eu^{3+} -doped nanoparticles.²⁵

3.2.2. BaFCl: Ce^{3+} , Tb^{3+} . Similar to the long-lived red emissions of Eu^{3+} ions, green luminescence of Tb^{3+} ions using Ce^{3+} ions as sensitizers has been observed in BaFCl nanoparticles. To overcome the low absorptions of parity forbidden f–f transitions of Tb^{3+} , enhanced PL output of Tb^{3+} ions is usually achieved *via* the sensitization by other Ln^{3+} ions (*e.g.*, Ce^{3+}) with an allowed electronic 4f–5d transition.^{23,26} As shown in Fig. 5(a), bright green luminescence upon irradiation at 254 nm with a 4 W hand-held UV lamp was observed. More importantly, the PL intensity of BaFCl: Ce^{3+} , Tb^{3+} nanoparticles in aqueous solution remained unaltered under UV irradiation for 24 h, indicative of the high photostability of the sample. Such bright green luminescence of BaFCl: Ce^{3+} , Tb^{3+} has not been reported before. Fig. 5(b) displays the excitation ($\lambda_{\text{em}} = 542$ nm) and emission ($\lambda_{\text{ex}} = 265$ nm) spectra of BaFCl: Ce^{3+} (3 at.%), Tb^{3+} (1 at.%) nanoparticles in aqueous solution. The emission spectrum exhibits typical emission bands at 486, 542, 582, 620, and 644 nm that correspond to the 5D_4 to 7F_6 , 7F_5 , 7F_4 , 7F_3 , and 7F_2 transitions of Tb^{3+} ions with the dominant emission of the $^5D_4 \rightarrow ^7F_5$ transition. The strong excitation band in the wavelength range between 230 and 320 nm corresponds to the 4f \rightarrow 5d absorption of Ce^{3+} ions, which shifts to the red in comparison with that previously reported for CeF_3 : Tb and LaF_3 : Ce , Tb nanoparticles.^{16,27} Due to the exposure of the 5d orbitals of Ln^{3+} ions to the environment, the absorption band of Ce^{3+} is susceptible to the crystal field. The energy transfer process from Ce^{3+} to Tb^{3+} is schematically shown in Fig. 5(c). The Ce^{3+} ions are firstly excited to the 5d orbitals by the absorption of UV light, subsequent transfer of energy to Tb^{3+} ions, and then radiative emissions from 5D_4 of Tb^{3+} are observed in the green region.

It is well known that for biological labeling, green emissions of Tb^{3+} under UV excitation would inevitably suffer from the interference of scattered lights and short-lived autofluorescence from cells and tissues, which result in a lower signal-to-noise ratio.²⁸ To completely avoid such interferences and improve the

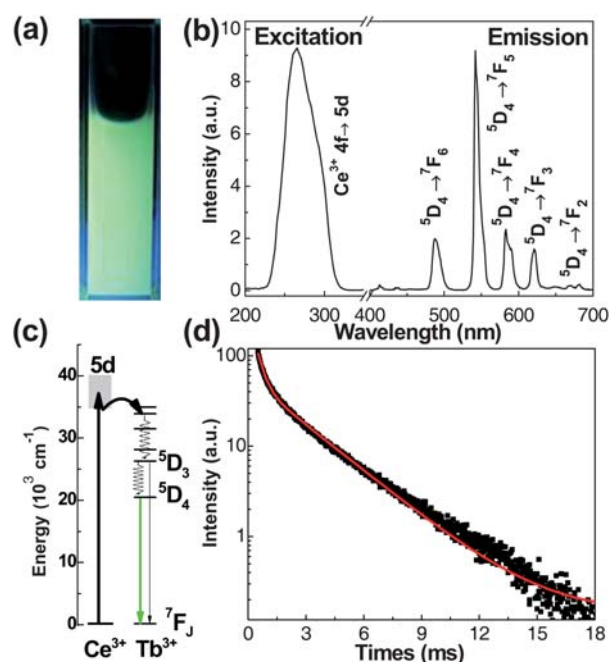


Fig. 5 (a) PL photograph of BaFCl: Ce^{3+} (3 at.%), Tb^{3+} (1 at.%) nanoparticles in aqueous solution under irradiation at 254 nm with a 4 W hand-held UV lamp; (b) the excitation (left, $\lambda_{\text{em}} = 542$ nm) and emission (right, $\lambda_{\text{ex}} = 265$ nm) spectra of the sample; (c) energy level scheme of Ce^{3+} and Tb^{3+} ions and energy transfer process; (d) PL decay from 5D_4 of Tb^{3+} ions under excitation at 265 nm.

detection sensitivity, the technique of time-resolved (TR) luminescence detection combined with the long-lived luminescence species has been employed.⁹ To prove the feasibility of BaFCl: Ce^{3+} , Tb^{3+} nanoparticles in TR detection, the luminescence decay of the 542 nm emission was measured under the excitation at 265 nm (Fig. 5(d)). Similar to that of Eu^{3+} ions, the decay curve can also be fitted with a biexponential function, and the fitted lifetimes were 2.54 (60%) and 0.32 ms (40%), respectively. Likewise, the short component of PL lifetime may be induced by the non-radiative energy transfer from Tb^{3+} to the surface defects. The PL lifetime of Tb^{3+} is much longer than that of autofluorescence and scattering lights that last only several nanoseconds, thus the short-lived background luminescence can be effectively inhibited if a proper delay time is set in the TR detection.

3.3.3. BaFCl: Nd^{3+} . For *in vivo* imaging, biolabels with both the excitation and emission bands in the NIR region have been proposed to be more attractive, since biological tissues are rather transparent in the NIR spectral range and suffer from less damage under excitation in such range.²⁵ To meet these requirements, Nd^{3+} ions with the excitation and emission both in the NIR region were doped in BaFCl nanoparticles. Fig. 6 shows the emission spectrum of BaFCl: Nd^{3+} (1 at.%) nanoparticles in aqueous solution under laser excitation at 808 nm. The spectrum exhibits three typical emission bands of Nd^{3+} at 886, 1055 and 1328 nm, corresponding to the $^4F_{3/2} \rightarrow ^4I_{J/2}$ ($J = 9, 11, 13$) transitions, respectively, with the most intense emission peak centered at 1055 nm. The luminescence decay of $^4F_{3/2}$ (1055 nm) under the excitation at 808 nm was measured at RT

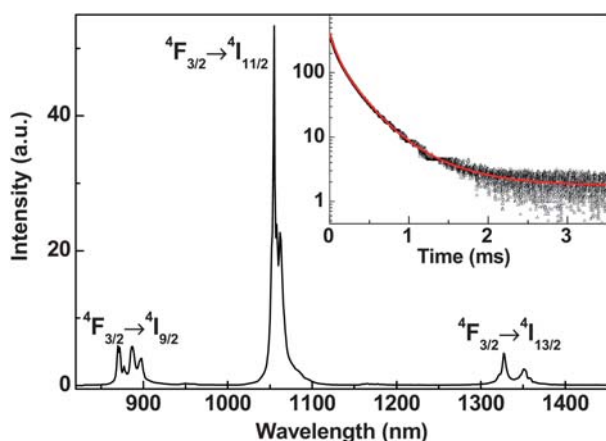


Fig. 6 RT emission spectrum of BaFCl:Nd³⁺ (1 at.%) under laser excitation at 808 nm. The inset shows the PL decay from ⁴F_{3/2} of Nd³⁺ under the excitation at 808 nm.

(inset of Fig. 6). The decay curve can be fitted well with a triple exponential function, and the fitted lifetimes were 0.58 (0.6%), 0.24 (2.4%) and 0.07 ms (97%), respectively. The much shorter lifetime of Nd³⁺ compared to that of Eu³⁺ and Tb³⁺, is ascribed to its much narrower energy gap between the emissive state (⁴F_{3/2}) and its next low-lying state (⁴I_{15/2}).⁹ Because both the excitation and major emission peaks of Nd³⁺ are present within the “optical window” (spectral range of 650–1300 nm) of cells and tissues and its luminescence lifetime is much longer than that of autofluorescence of organism and scattered light, BaFCl:Nd³⁺ nanoparticles might be very promising to be used as NIR fluorescent labeling agents for ultra-sensitive bioassays and bioimaging.

4. Conclusions

A simple one-step solvothermal method by employing PAA as a capping agent has been developed to synthesize water-soluble and surface-functionalized BaFCl:Ln³⁺ nanoparticles. The synthesized nanoparticles are well dispersed with a size of 20–40 nm, and their surfaces were effectively capped with the PAA layer having a thickness of 5–15 nm. Through doping different lanthanide ions, intense and long-lived red, green, and NIR emissions have been realized. By means of Eu³⁺ as a probe, we conclude that the doped Eu³⁺ ions occupy a distorted lattice site close to the surface. Intense green luminescence of Tb³⁺ sensitized by Ce³⁺ and NIR emissions of Nd³⁺ have been observed for the first time in BaFCl nanoparticles. The Ln³⁺-doped BaFCl nanoparticles featuring excellent water dispersibility, surface functionalization, intense and long-lived red, green and NIR luminescence, are highly promising for applications in fluorometric immunoassay, DNA hybridization, and bioimaging.

Acknowledgements

This work is supported by the Hundreds of Talents and Knowledge Innovation Programs of the Chinese Academy of Sciences (CAS) for Key Topics (No. KJCX2-YW-358) and Young Scientists, Instrument Developing Project of CAS (No. YZ200712), the NSFC (Nos. 10804106 and 10974200), the 973 and 863 programs of MOST (Nos. 2007CB936703 and 2009AA03Z430), Fujian Provincial Science Fund for Distinguished Young Scholars (No. 2009J06030), and the Key Project of Science and Technology Foundation of Fujian Province (No. 2007I0024).

Notes and references

- 1 E. Schrock, S. duManoir, T. Veldman, B. Schoell, J. Wienberg, M. A. FergusonSmith, Y. Ning, D. H. Ledbetter, I. BarAm, D. Soenksen, Y. Garini and T. Ried, *Science*, 1996, **273**, 494.
- 2 P. R. Diamente and F. C. J. M. van Veggel, *J. Fluoresc.*, 2005, **15**, 543.
- 3 L. Y. Wang, R. X. Yan, Z. Y. Hao, L. Wang, J. H. Zeng, H. Bao, X. Wang, Q. Peng and Y. D. Li, *Angew. Chem., Int. Ed.*, 2005, **44**, 6054.
- 4 F. Wang, W. B. Tan, Y. Zhang, X. P. Fan and M. Q. Wang, *Nanotechnology*, 2006, **17**, R1.
- 5 P. S. Ghosh, C. K. Kim, G. Han, N. S. Forbes and V. M. Rotello, *ACS Nano*, 2008, **2**, 2213.
- 6 L. Wang and W. H. Tan, *Nano Lett.*, 2006, **6**, 84.
- 7 J. Kim, Y. Piao and T. Hyeon, *Chem. Soc. Rev.*, 2009, **38**, 372.
- 8 F. Wang, X. J. Xue and X. G. Liu, *Angew. Chem., Int. Ed.*, 2008, **47**, 906.
- 9 J. C. G. Bunzli and C. Piguet, *Chem. Soc. Rev.*, 2005, **34**, 1048.
- 10 F. Wang and X. G. Liu, *J. Am. Chem. Soc.*, 2008, **130**, 5642.
- 11 X. Y. Chen, W. Zhao, R. E. Cook and G. K. Liu, *Phys. Rev. B: Condens. Matter Mater. Phys.*, 2004, **70**, 205122.
- 12 Q. Ju, Y. S. Liu, R. F. Li, L. Q. Liu, W. Q. Luo and X. Y. Chen, *J. Phys. Chem. C*, 2009, **113**, 2309.
- 13 M. N. Christof, *Angew. Chem., Int. Ed.*, 2001, **40**, 4128.
- 14 Z. Q. Li, Y. Zhang and S. Jiang, *Adv. Mater.*, 2008, **20**, 4765.
- 15 M. Wang, C. C. Mi, W. X. Wang, C. H. Liu, Y. F. Wu, Z. R. Xu, C. B. Mao and S. K. Xu, *ACS Nano*, 2009, **3**, 1580.
- 16 D. Y. Kong, Z. L. Wang, C. K. Lin, Z. W. Quan, Y. Y. Li, C. X. Li and J. Lin, *Nanotechnology*, 2007, **18**, 075601.
- 17 Z. Tang, Y. Wang, P. Podsiadlo and N. A. Kotov, *Adv. Mater.*, 2006, **18**, 3203.
- 18 T. R. Zhang, J. P. Ge, Y. P. Hu and Y. D. Yin, *Nano Lett.*, 2007, **7**, 3203.
- 19 F. Wang, Y. Zhang, X. P. Fan and M. Q. Wang, *Nanotechnology*, 2006, **17**, 1527.
- 20 P. R. Diamente, R. D. Burke and F. C. J. M. van Veggel, *Langmuir*, 2006, **22**, 1782.
- 21 J. P. Ge, Y. X. Hu, M. Biasini, C. L. Dong, J. H. Guo, W. P. Beyermann and Y. D. Yin, *Chem.–Eur. J.*, 2007, **13**, 7153.
- 22 L. Y. Wang, J. Bao, L. Wang, F. Zhang and Y. D. Li, *Chem.–Eur. J.*, 2006, **12**, 6341.
- 23 J. Q. Gu, J. Shen, L. D. Sun and C. H. Yan, *J. Phys. Chem. C*, 2008, **112**, 6589.
- 24 S. M. Chen, G. Z. Wu, Y. D. Liu and D. W. Long, *Macromolecules*, 2006, **39**, 330.
- 25 J. W. Stouwdam and F. C. J. M. van Veggel, *Nano Lett.*, 2002, **2**, 733.
- 26 J. C. Boyer, J. Gagnon, L. A. Cuccia and J. A. Capobianco, *Chem. Mater.*, 2007, **19**, 3358.
- 27 F. Wang, Y. Zhang, X. P. Fan and M. Q. Wang, *J. Mater. Chem.*, 2006, **16**, 1031.
- 28 J. C. G. Bunzli, *Chem. Lett.*, 2009, **38**, 104.